followed by a stop codon (Figure 1A and B). These mouse strains were termed *1 1 ^{20}* and *1 1 ^{22}*.

Expression of the truncated ATG16L1 CCD was verified by comparing western blots of tissue lysates from the *1 1 ^{20}* mice with littermate controls (Figure 1C). The ATG5 binding and CCD of ATG16L1 migrated at ~ 27 kDa compared to the ~ 70 kDa for full-length ATG16L1. As described by Mizushima et al [21], lysates from liver showed the α and β isoforms of ATG16L1 while the slower migrating β isoform predominated in muscle and brain. Full-length ATG16L1 was present in lysates obtained from littermate controls, but absent from tissues of *1 1 ^{20}* mice. It was not possible to detect the truncated CCD of the *1 1 ^{22}* mice, in whole tissue lysates. This may be because the epitope is lost, or the protein is highly unstable.

The size of the ATG16L1 complex generated in the mice was determined by gel filtration of cytoplasmic fractions isolated from homogenized liver (Figure 2). In control mice the α and β isoforms of ATG16L1 eluted in high molecular-mass fractions suggesting formation of a 300–600 kDa complex. Previous work has shown that elution of ATG16L1 in high molecular-weight fractions is dependent on ATG5 [21]. The presence of the ATG12–ATG5 conjugate in the same high molecular weight fractions as ATG16L1 suggested binding of ATG5 to the N-terminal ATG5-binding domain present in the CCD of

glutamate residues required for WIPI2 binding, and indirect evidence for binding to WIPI2 was provided by the elution of the 49-kDa WIPI2 protein in high molecular-mass factions ranging between 150 and 600 kDa. Analysis of the *1 1 2 0* and *1 1 22* mice was complex because the preparation of liver lysates appeared to result in limited proteolysis of CCDs, and the possible formation of dimers and trimers resistant to dissociation during SDS polyacrylamide electrophoresis (Fig. S1). The blots in Figure 2 show the elution profile of the 27-kDa CCD and the 25-kDa proteolytic products, which co-elute with multimers at 50 and 75 kDa (Fig. S1). The bulk of the CCD in the liver of *1 1 2 0* mice eluted over a broad range from ~300 kDa in fractions which also contained the ATG12–ATG5 conjugate and ATG5. As seen for control mice, WIPI2 was detected in high molecular-mass fractions eluting between ~400 kDa; however, levels of WIPI2 were less than seen for control, and a low molecular-mass fraction was also detected between 50 and 100 kDa. The CCD of *1 1 2 0* mice retained binding sites for ATG5 and WIPI2, and the elution profiles were consistent with assembly of complexes containing the CCD, ATG12–ATG5 and WIPI2. Unlike whole tissue lysates, it was possible to detect the CCD of the *1 1 22* mouse in fractions eluting from the gel filtration column. The CCD eluted over a broad ~300 kDa range in fractions that also contained ATG12–ATG5. The CCD of *1 1 22* mice lacks the E230 glutamate residue required for WIPI2. The blots show that unlike control mice and *1 1 2 0* mice, it was not possible to detect WIPI2 in high molecular-mass fractions, and WIPI2 eluted between 50 and 100 kDa. The results from this indirect assay based on the size of ATG16L1 complexes suggest that the CCD of *1 1 22* assembles with ATG12–ATG5 through the ATG5 binding domain, but does not bind strongly to WIPI2.

The ability of cells isolated from the mice to activate autophagy was tested by western blot of autophagy substrates SQSTM1/p62 (sequestosome 1) and LC3, and by following formation of LC3 puncta after starvation in Hanks balanced salt solution (HBSS) (Figure 3A-C). Mouse embryonic fibroblasts (MEFs) from mice lacking ATG16L1 (*1 1 -/-*) were used as an autophagy-negative control. MEFs from control mice expressed the α and β isoforms of ATG16L1 which were absent from *1 1 -/-*, *1 1 22* and *1 1 2 0* MEFs, whereas *1 1 2 0* MEFs showed the smaller band expected at 27 kDa (data not shown). *1 1 -/-* MEFs showed defects in autophagy indicated by the expression of high levels of the autophagy substrate SQSTM1, and an inability to generate lipidated LC3-II (Figure 3A) after starvation. MEFs expressing ATG16L1^{E226} also expressed high levels of SQSTM1 and were unable to generate lipidated LC3-II showing that loss of E230 resulted in defects in autophagy. This supported the observation that MEFs (Figure 3B) and skin fibroblasts (Figure 3C) from *1 1 22* mice were unable to generate LC3 puncta following starvation. In contrast, cells expressing full-length ATG16L1, or expressing the CCD but lacking the WD domain (ATG16L1^{E230}) were able to activate autophagy, indicated by low basal levels of SQSTM1 and generation of LC3 puncta in response to HBSS (Figure 3B,C). Taken together, these results showed that autophagy requires the E226 and E230 glutamate residues in the CCD needed for WIPI2 binding, but, as reported previously [19], autophagy did not require the WD domain. The role played by the WD domain during LAP was analyzed by incubating bone marrow-derived macrophages (BMDMs) from the mouse strains with Pam3CSK4 (a mimic of bacterial lipopeptides)-coupled polystyrene beads to follow LC3 translocation to phagosomes (Figure 3D). LC3 was recruited to phagosomes in macrophages from control 4aolasE22ve 4acrophages fr

reported previously [12,23] these observations indicate that the WD domain is required for LAP in myeloid cells, and confirmed that the *1 1 20* mouse would provide a LAP-deficient mouse model to study the role played by LAP in maintaining tissue homeostasis .

The LAP-deficient *1 1 20* mice survived the postnatal lethality seen in *1 1 -/-* mice [15], and were similar in size and weight to littermate controls and grew at comparable rates (Figure 4A, B). *1 1 20* mice were born with Mendelian frequency with reproductive organs of normal size, and were fertile with a reproductive capacity comparable to controls (data not shown). The survival rate and litter sizes of *1 1 20* mice were similar to wild-type mice with life spans of at least 24 months (data not shown). The majority of *1 1 22* mice also survived postnatal lethality, but most grew slowly (Figure 4A, B) and died within 5–7 months of age.

LAP-deficient mice generated by *2/ -* -driven loss of from macrophages, monocytes and neutrophils (3) develop

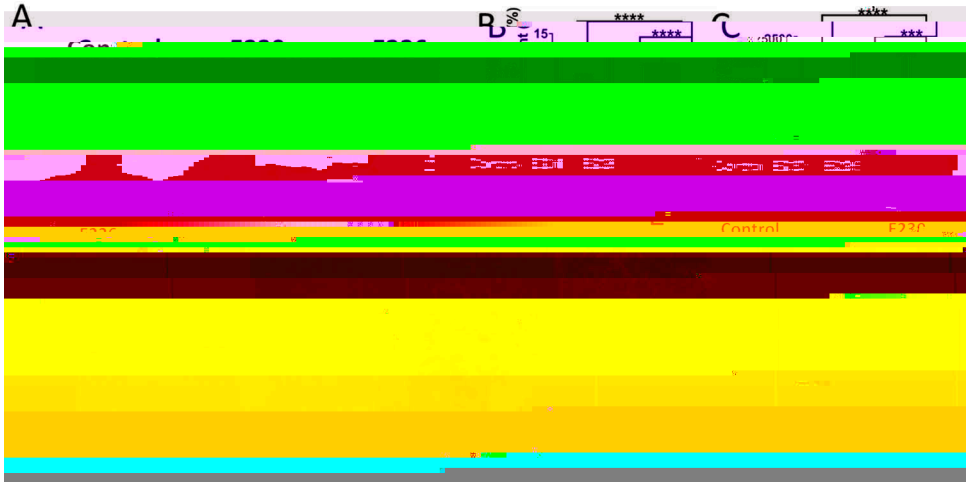

Figure 5. Analysis of autophagy substrates in liver. Panel (A) Representative livers at ~2 months (scale bar: 1 cm). (B) Liver weight expressed as body weight at 2–3 months of age. E230 (*Atg16l1*^{E230}) n = 9, control n = 8; E226 (*Atg16l1*^{E226}) n = 9, control n = 7. (C) GPT/ALT in serum from mice aged between 2–3 months. E230 (*Atg16l1*^{E230}) n = 7, control n = 5; E226 (*Atg16l1*^{E226}) n = 5, v control n = 5. (D) Western blot of liver lysates from 3 representative mice. Membranes strips taken from the appropriate molecular weight range were analyzed separately using the indicted antibodies. (E) Representative histochemical sections o immunostained for SQSTM1. Enlarged regions of interest are shown in the lower panel. Arrows: SQSTM1 inclusions. In all figures data from littermate con E230 and E226 were pooled. Statistical analysis was done by unpaired t test. Error bars represents ±SEM. ****-P < 0.0001, ***-P < 0.001; ns, non-significar magnification 40X, scale bars: 50 µm.

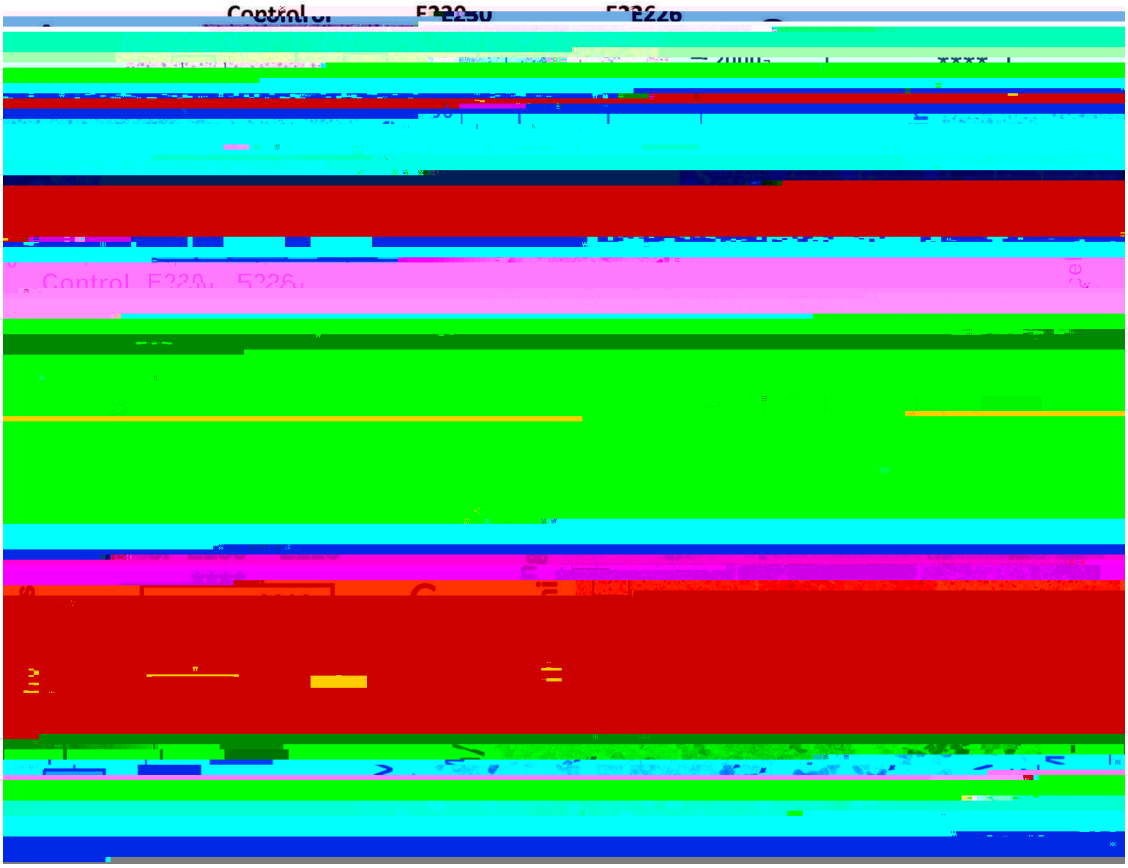

Figure 6. Analysis of liver homeostasis. (A) Representative images of H&E-stained sections of livers. Boxed regions of interest are enlarged in lower panels. graph represents comparative circumferences of hepatocytes (n = 10) across the indicated strains (n = 3 for all the strains). (B and C) Representative histoc sections of liver immunostained with antibodies against MKI67/Ki67 (B) or ITGAM/Cd11b (C). Regions of interest are enlarged and shown in lower panels. indicate positive staining. Bar graphs show number of positive cells (C) or percent positive cells (B). Five different zones for each liver section were analyzed (r all the strains). Data across littermate control mice for E230 and E226 were pooled. Statistical analysis was done by unpaired t test. Error bars represents ****-P < 0.0001, *-P < 0.1. Magnification 20X, scale bars: 50 µm.

Liver inflammation was also evident from increased infiltration of ITGAM/CD11b-positive leukocytes (Figure 6C). In contrast, livers from the $1\ 1^{20}$ mice showed little sign of damage. A

Mice with systemic loss of ATG16L1 from all tissues (*1* $^{-/-}$) die at birth from a suckling defect[15]. This raised the question of how the *1* *1* ^{22} mice, which appear autophagy-defective, survive neonatal lethality. Neonatal lethality in 5 $^{-/-}$ mice can be reversed by brain-specific re-expression of ATG5[24]. These rescued mice (-) lack ATG5 and autophagy in non-neuronal tissues and develop multiple organ abnormalities with a

filtration was repeated for brain lysates (Figure 10). As seen in liver, ATG16L1 in control mice eluted in high molecular-mass fractions suggesting formation of a 300- to 600-kDa complex.

plants and humans contains over half the amino acids of the 66-kDa protein [21]. Gel filtration analysis suggested that full-length ATG16L1 formed a 300- to 600-kDa complex in liver and brain. The CCDs of the $1\ 1^{20}$ and

level of autophagy is provided in Figure 3A where accumulation of SQSTM1 in MEFs from *1 1* ^{22} appeared lower than following complete loss of ATG16L1, and there was a feint band for LC3-II. In addition, the requirement for WIPI2 binding to ATG16L1 to initiate autophagy may differ between brain and peripheral tissues. Support for this is provided by gel filtration analysis which suggested that binding of WIPI2 to the E230 glutamate residue in the CCD of ATG16L1 occurred in liver, but binding was much weaker in brain.

The phenotype of the *1 1* ^{22} mouse was very similar to the 5-null mouse described by Yoshii et al. [24] where ATG5 expression was restored in the brain of $^{-/-}$ mice. In common with *1 1* ^{22} mice, the 5-null mouse survived neonatal lethality but grew slowly and showed SQSTM1 accumulation in peripheral tissues, particularly liver and muscle. The -null mice were sterile and have

macrophage cultures at a ratio of 10:1 (bead/cell) for 1.5 h before being fixed and the location of LC3 analyzed by immunofluorescence microscopy.

Dissected tissue was snap-frozen in liquid nitrogen, ground to a fine powder under liquid nitrogen and lysed in RIPA buffer (150 mM sodium chloride, 1% TritonX-100 [Sigma, P1379-1L], 0.5% sodium deoxycholate [Sigma, D-5670], 0.1% sodium dodecyl sulfate [Fisher Bioreagents, BP166-500], 50 mM Tris, pH 8.0) containing protease (Sigma, P8340) and phosphatase (Sigma, P5726) inhibitors followed by homogenization and freeze thaw. Samples were clarified by centrifugation (10,600 g, 10 min at 4°C). Supernatants containing 10 ug protein were boiled in Laemmli buffer followed by SDS-PAGE using 412% gradient gels (Expedeon, NBT41212). The resolved proteins were electro-blotted onto nitrocellulose membrane (Bio-Rad, 1,620,115), blocked (5% skimmed milk in 1X TBS [50mM Tris (pH 7.5), 150mM NaCl], 1 h, room temperature) and then probed first with appropriate primary (ATG16L1 [MBL, M150-3], SQSTM1/p62 [Abcam, ab91526], GAPDH [Abcam, ab9482] and LC3A/B [Cell Signalling

[31] Boada-Romero E, Letek M, Fleischer A, et al. TMEM59 defines a novel ATG16L1-binding motif that promotes local activation of LC3. Embo J 2013;32(4):566-582.
[32] Hu J, Li G, Qu L, et al. TMEM166/EVA1A interacts with ATG16L1 and induces autophagosome formation and cell death. Cell Death Dis 2016;7(8):e2323.
[33] Conrad M, Brielmeier M, Wurst W, et al. Optimized vector for conditional gene targeting in mouse embryonic stem cells. Biotechniques 2003;34(6):1136-1138, 40.
[34] Mayer U, Saher G, Fässler R, et al. Absence of integrin α7 causes a novel form of muscular dystrophy. Nat Genet. 1997;17(3):318-323.
[35] Nagy A, Rossant J, Nagy R, et al. Derivation of completely cell culture-derived mice from early-passage embryonic stem cells. Proc Natl Acad Sci 1993;90(18):8424-8428.